2010 IEEE/ASME International Conference on
Advanced Intelligent Mechatronics
Montréal, Canada, July 6-9, 2010

Coalescence Constraints for Inkjet Print Mask Optimization

J. William Boley, Kartik B. Ariyur, George T.-C. Chiu, *Members, ASME*

Abstract— **A print mask is a unique way of controlling the firing sequence of nozzles in inkjet printing. It is desirable to design a print mask which maximizes throughput while maintaining desired image quality. This can be formulated as an optimization problem where the objective is to maximize throughput by minimizing printing time subject to image quality constraints under uncertainties and variations in the printing process. Coalescence is an important image quality artifact. This paper outlines the development of a coalescence model, which can be used as an image quality constraint in finding an optimal print mask. The proposed coalescence model computes the probability of coalescence as a function of time between two adjacent drops. Monte Carlo simulation is used based on experimentally obtained distributions of model parameters. Given an acceptable coalescence probability the minimum printing time between adjacent drops can be determined, which translates to a minimum distance between pixels in a print mask that can be printed on the same pass.**

I. Introduction

Inkjet printing has been shown to be a fast and inexpensive means of fabricating electrical devices at the MEMS scale [1, 2]. This technology is an attractive means of fabrication because of the low amount of energy and time required for production when compared to other techniques such as photolithography [3]. Advances in drop-on-demand devices have been steady ever since the 1970s [2]. Such advances have enabled the fabrication of MEMS devices such as printed strain gages and transistors [1, 2]. With a wide variety of printable materials and substrates, the possibilities of applications for inkjet technology are endless.

The two most widely used methods for drop formation in inkjet printing are piezoelectric and thermal actuation [2]. Piezoelectric drop formation devices usually consist of a standing column of fluid inside a tube, which has pressure pulses induced upon it by a voltage controlled piezoelectric material. These pressure pulses induce waves in the standing column of fluid, which are responsible for the formation of the drop. Thermally actuated drops are similar to that of piezoelectric drops in that the drops are generated through waves induced in a standing fluid. The only difference with thermal actuation is that the waves are produced by the formation and collapse of a vapor bubble in the fluid at the interface of a heater within the mechanism [4].

Inkjet print-heads typically contain arrays of nozzles [5]. The ability to produce simultaneous drops from multiple nozzles gives way to shorter fabrication time. Image quality is directly related to the accuracy in which drops are deposited onto the substrate, i.e. drop placement accuracy. For arrays of multiple nozzles, the drop placement accuracy can be affected by the variations due to nozzle fabrication, drop trajectories, and media advance. There has been some effort in recent years with improving inkjet print quality by controlling the firing timing in nozzle arrays [5-7]. A print mask is a unique way of controlling the firing sequence of nozzles in inkjet printing.

As such, it is desirable to design a print mask which maximizes throughput while maintaining desired image quality. This can be formulated as an optimization problem where the objective is to maximize throughput by minimizing printing time subject to image quality constraints under uncertainties and variations in the printing process.

Yen et al. [5] incorporated the bleeding between two adjacent pixels and the limitations of firing frequency in print mask design by disallowing concurrently firing physically adjacent nozzles. This constraint reduces the print artifacts such as drop coalescence on non-porous substrates and bleeding in porous media.

Coalescence occurs between two drops in contact because the surface energy between the drop and the substrate is not enough to overcome the surface energy between the drops. As a result, the surface tension of the drops causes them to merge into one another as shown in Fig. 1. In Fig. 1, the left image shows two drops in contact with one another while resting on the substrate just prior to coalescence. The image on the right shows the result of the two drops coalescing into one larger drop.

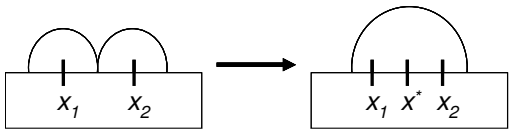

Fig. 1. schematic of two adjacent drops on a substrate (left) and coalescing into one larger drop (left).

Coalescence becomes an issue in printing when the application requires adjacent drops to overlap on the substrate. One example of such an application is in the printing of electrical circuits onto non-porous substrates such as oxidized silicon or glass. Printing electrical circuits requires the drops to overlap to maintain continuity. However, the incidence of coalescence between two adjacent drops pulls them away from neighboring drops that may result in an open circuit.

Although disallowing adjacent nozzles to be fired at the

same time to avoid coalescence makes sense intuitively, the question of necessity and sufficiency comes to mind. For example, when the surface energy between the substrate and the drop is much larger than that of the adjacent drops, firing adjacent nozzles at the same time may not result in coalescence, thus rendering the constraint unnecessary. On the other hand, the wide spreading of drops on the substrate may require that the spacing between simultaneously fired nozzles be larger than that of two nozzles, thus causing the constraint to be insufficient [8].

To this date, extensive literature searches have found no models to physically describe the occurrence of coalescence between two drops on a flat substrate. This paper outlines the development of a coalescence model, which can be used as an image quality constraint in finding an optimal print mask. The remainder of the paper is organized as follows. Print mask and the corresponding optimization problem are described in the next section. The coalescence modeling is discussed in section III. Numerical results are presented in section IV followed by concluding statements.

II. Print Mask

In general, print masks are applicable when printing with a cartridge containing multiple nozzles as shown in Fig. 2. Printing with the ability to fire all nozzles at once while passing over the media would result in the minimum printing time. However, due to quality considerations, sometimes it is preferred to pass over a given pixel on the media more than once, which is known as multiple pass printing [5]. Let n be the total number of times that the cartridge passes over any pixel on the media, referred to as the total number of passes. In multiple pass printing, the printer cartridge sweeps over the media in the print-head scan direction until it has reached the limits of the image. Then the media advances in the media advance direction a constant distance known as the nozzle advancement distance d, defined as

$$d = \frac{k}{n} \cdot \frac{1}{dpi}, \tag{1}$$

where *dpi* stands for dots per inch, which is the nozzle resolution. From (1) it is evident that the restrictions $n \leq k$ and n is an integer factor of k must hold.

Without loss of generality it can be assumed that each pixel on the media is a square with each side being of length 1/*dpi*. For simplicity, this paper assumes that each pixel of the image will receive at most one drop of ink. The logic can be extended to account for multiple drops of ink per image pixel [5]. If the image is of pixel size M by N, then one can think of a print mask as being an M by N matrix of integers from one to n, thus assigning a pass number for each pixel of the image. However, in practice this large M by N matrix can be the augmentation of a single, smaller matrix. This smaller

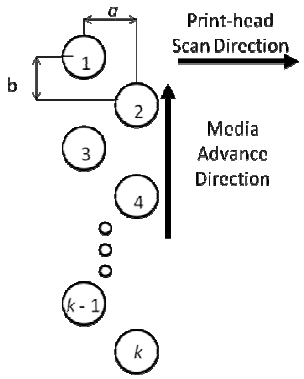

Fig. 2. Schematic of an inkjet nozzle array containing k nozzles and defining their relative spacing with the print-head scan direction and media advance direction defined relative to the nozzle array.

matrix is the print mask, denoted *PM*. Each *PM* gives a correspondence between a nozzle on the print-head and a pixel on the image.

Figure 3 illustrates the use of a print mask in a 2-pass print mode. Figure 3(a) is the image to be printed using print mask Fig. 3(b). Each pixel of Fig. 3(b) contains a "1" or a "2", which means that, if required by the image in Fig. 3(a), then ink will be deposited on the first or second pass, respectively. To print this image, three nozzles of the print-head sweep across the image in the positive print-head scan direction for its first pass to produce Fig. 3(c).

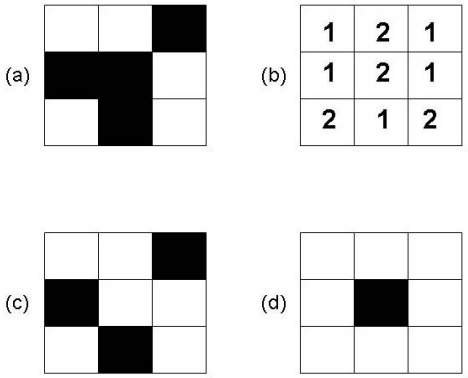

Fig. 3. Print mask (a) Image to be printed, (b) Print mask, (c) Image printed during first pass, (d) Image printed during second pass.

Upon reaching the end of the image, the media advances three pixels in the media advance direction before the next three nozzles of the print-head pass back over the image to print Fig. 3(d). As one can see, the logical OR operation of Fig. 3(c) and (d) results in Fig. 3(a).

Figure 4 illustrates the implementation of a *PM*. Figure 4(a) is the word "HI", which is a 9 pixel by 10 pixel image. Figure 4(b) is the binary representation of Fig. 4(a), where a "1" denotes ink should be deposited on the pixel and "0" denotes no ink should be deposited on the pixel. Figure 4(c) is the 2 by 2 *PM*. Figure 4(d) is the augmented 9 by 10 canvas generated by the *PM*. The image, Fig. 4(e) is the

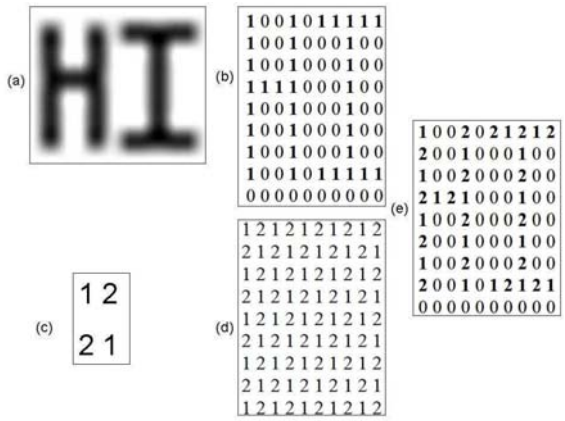

Fig. 4. Print mask implementation (a) Input image, (b) Binary image, (c) Print mask, (d) Canvas, (e) Output image with pass numbers.

result of the logical AND operation between Fig. 4(b) and (d). It should be noted that the bottom *k*/*n* nozzles sweep over the top *k*/*n* rows of pixels of the media with the first print-head scan.

Given a specific printing system, the process of selecting an appropriate *PM* can be formulated as an optimization problem, where the objective is to maximize throughput while maintaining acceptable image quality. Given the following printing system parameters:

- Print-head scan velocity
- Nozzle resolution, *dpi*
- Total number of nozzles, *k*
- Distance between nozzle columns of nozzle array, *a*
- Maximum nozzle firing frequency

an optimal *PM* will minimize the printing time subjected to acceptable image quality constraints. For a given print-head scan velocity, minimizing printing time implies maximizing the nozzle advancement *d* described in (1), which is equivalent to minimizing *n*.

To solve the optimization problem, a properly formulated image quality constraint will need to be derived. In this work, image quality constraints to avoid coalescence will be discussed. The next section proposes a model for determining the probability of coalescence occurring; whereby choosing an acceptable coalescence probability reduces the number of admissible print masks.

III. Coalescence Model

Assume each drop is circular with a time (*t*) dependent radius *r*(t), and a center location (*x*, *y*). The size, *r*(*t*) of a drop after impacting the substrate can be characterized by a relatively fast spreading and receding response and a slow contraction due to evaporation [8-25]. For the remainder of the paper, we will assume that the drop has stabilized after its spreading and receding has subsided. Figure 5 shows the top view of two drops on a substrate, where subscript 1 denotes the first drop and subscript 2 denotes the second drop deposited some time after the first drop stabilized. We assume that coalescence will occur when the wetted area occupied by the second drop intersects with the wetted area occupied by the first drop. Conversely, coalescence will not occur if

$$0 < \sqrt{(x_1 - x_2)^2 + (y_1 - y_2)^2} - (r_1(t) + r_2(t)), \qquad (2)$$

for all time after the first drop has stabilized.

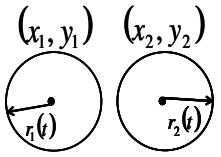

Fig. 5. Top view of two drops on a substrate.

There are two key factors in determining when (2) occurs. One factor comes from the spreading and receding of the drop once it has impacted the substrate. This phenomenon contributes only to the dynamics of $r_2(t)$ because it is assumed that the spreading and receding dynamics of the first drop have stabilized when the second drop lands. The second factor is the evaporation of a sessile drop on a solid surface, which occurs at a much larger time scale than the spreading and receding dynamics and only affects the dynamics of $r_1(t)$.

For the modeling of the second drop impacting the substrate, as a conservative lower bound, (2) is always satisfied if

$$0 < \sqrt{(x_1 - x_2)^2 + (y_1 - y_2)^2} - \left(r_1(t) + \max_t r_2(t)\right), \qquad (3)$$

where $\max_t r_2(t)$ is the maximum of $r_2(t)$ for all time. This is a conservative approach because the first drop will be evaporating during the spreading process of the second drop. However, this approximation is valid since the collision dynamics are faster than the evaporation dynamics [10, 21].

G. German et al. [13] review many existing models for finding the maximum value of $r_2(t)$. These models range from that of an algebraic empirical nature to that a second order nonlinear theoretical nature. We will be using the semi-empirical algebraic model proposed by Pasandideh-Fard et al. [15], which has been shown to closely match experimental data [13]. Let W_e be the typical Weber number of a drop falling in air, Θ_a the contact angle of the advancing fluid on the substrate, R_e the Reynolds number of a drop falling in air, D_0 the drop diameter in air, ρ the density of the drop, V_0 the velocity of the drop prior to impact, σ the surface tension of the drop, and μ the viscosity of the drop. Then the maximum radius of the second drop can be found by

$$\max_t r_2 = \frac{\beta_m D_0}{2}; \tag{4}$$

where

$$\beta_m = \sqrt{\frac{We+12}{3(1-\cos\theta_a)+4\left(We/\sqrt{\mathrm{Re}}\right)}},$$

$$W_e = \frac{\rho D_0 V_0^2}{\sigma},$$

and

$$R_e = \frac{\rho D_0 V_0}{\mu}.$$

Although the Pasandideh-Fard model is used in this study, any other model can be used with the proposed approach.

In order to capture the dynamics of the radius of the first drop due to evaporation, the constant contact angle model proposed by Picknett et al. [21] will be used. Let $W(t)$ be the mass of the liquid drop, Θ_0 the contact angle of stabilized drop on the substrate, α the binary mass diffusion constant of the drop in air, c_0 the vapor mass concentration of the printed material close to the drop, and c_i the vapor mass concentration of the printed material far from the drop. Then the radius of the wet area of the first drop as a function of time can be found by

$$r_1(t) = E\left(W(t)/\rho\right)^{\frac{1}{3}} \cdot \sin\theta_0; \tag{5}$$

where

$$\frac{dW}{dt} = -qE(C/r)W^{\frac{1}{3}}\Big/ 2\rho^{\frac{1}{3}}, \tag{6}$$

$$E = 3\Big/\left\{\pi(1-\cos\theta_0)^2(2+\cos\theta_0)\right\},$$

$$q = 4\pi\alpha(c_0 - c_i).$$

The ratio C/r can be empirically determined as

$$C/r = 0.6366\theta_0 + 0.09591\theta_0^2 - 0.06144\theta_0^3,$$

for $0 \le \Theta_0 \le 0.175$ radians, or for $0.175 \le \Theta_0 \le \pi$ radians,

$$C/r = 0.00008957 + 0.6333\theta_0 + 0.1160\theta_0^2 - 0.08878\theta_0^3 + 0.01033\theta_0^4.$$

In (5), W(t) is found by numerically solving (6) with a random initial condition due to variation in the initial volume.

The coalescence model defined in (3) also depends on drop placement accuracy. Experiments were conducted to characterize the variation distribution for the drop placement in the x and y directions for an array of nozzles used in the Purdue inkjet printing lab. Figure 6 shows an example of a grid of drops printed from one nozzle. The material printed was a 300mM concentration of Pd hexadecanethiolate on a steel substrate with an upper layer of heat curable epoxy (20 – 3300 high temperature and thermal shock epoxy from Epoxies, Etc.) applied with a razor blade. The image was taken with a high resolution digital microscope (Keyence VH-600 with a VH-Z20 lens at 50X magnification).

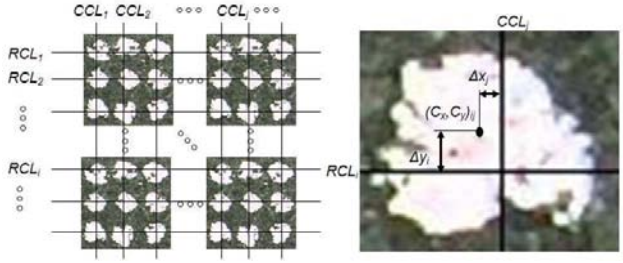

Fig. 6. (a) Printed grid of drops from a single nozzle and (b) Close-up of a single drop in the printed grid.

The centroid, $(C_x, C_y)_{ij}$ of drop ij in Fig. 6 can be found by using the methods described in Bernal et al. [26]. The x coordinate of the jth column center line CCL_j can be computed by

$$CCL_j = \frac{\sum_{i=1}^{p_j}(C_x)_{ij}}{p_j},$$

where p_j is the total number rows in the jth column. Similarly, the y coordinate of the ith row center line RCL_i can be computed by

$$RCL_i = \frac{\sum_{j=1}^{p_i}(C_x)_{ij}}{p_i},$$

where p_i is the total number of columns in the ith row. Then the drop placement variation for drop ij can be computed by

$$\Delta x_{ij} = (C_x)_{ij} - CCL_j \text{ and } \Delta y_{ij} = (C_y)_{ij} - RCL_i.$$

Variation in drop placement error, Δx and Δy can be empirically obtained by finding the distribution of Δx_{ij} and Δy_{ij}, respectively.

For each time (t) after stabilization of the first drop, given the distribution of Δx and Δy, Monte Carlo simulation can be performed to compute the probability of the occurrence of coalescence using (3), where $\max_t r_2$ is obtained from (4)

and $r_1(t)$ from (5). This resulting probability gives a constraint on the firing time between nozzles on the print-head. Since the print-head scan speed is known, the firing timing constraint becomes a constraint on adjacent values in the optimal *PM*.

Although Monte Carlo simulation is used in this study given the experimentally obtained drop placement error distribution, more analytical approaches can be employed if theoretical distributions of the random variables are available.

IV. Numerical Results

Printing water on glass will be used to demonstrate the utility of the proposed model. TABLE I shows a summary of the specific parameters used in this example. The parameters given in TABLE I are actual values of the inkjet system in the Purdue lab. In regards to the water vapor concentrations, c_0 is the saturated water vapor concentration at 20°C while c_i is assumed to be dry air.

TABLE I
Summary of Simulation Parameters

Parameter	Quantity
Density (kg/m^3)	1000
Viscosity (Pa*s) @ 20°C	0.001
Surface Tension (N/m) @ 20°C	0.07288
Drop Volume (m^3)	5 x 10^{-14}
D_0 (m)	4.57 x 10^{-5}
V_0 (m/s)	4.8
Reynolds Number	219.4
Weber Number	14.45
Θ_a (degrees)	27
Θ_0 (degrees)	27
dpi (1/inch)	360
D (m^2/s) @ 20°C	0.26 x 10^{-4}
c_0 (kg/m^3)	0.023
c_i (kg/m^3)	0

When dealing with drops printed on a substrate, coalescence can occur between drops printed adjacently in the vertical direction, the horizontal direction, or along the diagonal. For this simulation, coalescence is only considered between two drops adjacent in the vertical direction, printed from different nozzles. Because of circular symmetry the result is applicable for both horizontal and diagonal directions. Figure 7 shows the Monte Carlo simulation results using the model. Forty equally spaced time samples from 0 seconds to the total drying time of an average drop are used. For each time sample, 100,000 uniformly selected random samples were taken from the distributions for x_1, x_2, y_1, y_2, and r_1. In general, the maximum value of r_2 may have a distribution induced by the potential distribution of D_0 and V_0; for this example nominal values are used. The x axis of Fig. 8 represents the time elapsed between when the first drop stabilizes and the when the second drop is deposited. The y axis is the probability that the two drops will coalesce. As expected, the probability decreases as time increases. For example, one can say with probability one that after approximately 580 milliseconds there will be no coalescence between these drops.

Using this model, given an acceptable coalescence probability the minimum printing time between adjacent drops can be determined. Given the minimum print time, the print-head scan speed, distance between nozzle columns in a nozzle array, and the nozzle resolution, one can then compute the minimum distance between pixels in a print mask that can be printed on the same pass.

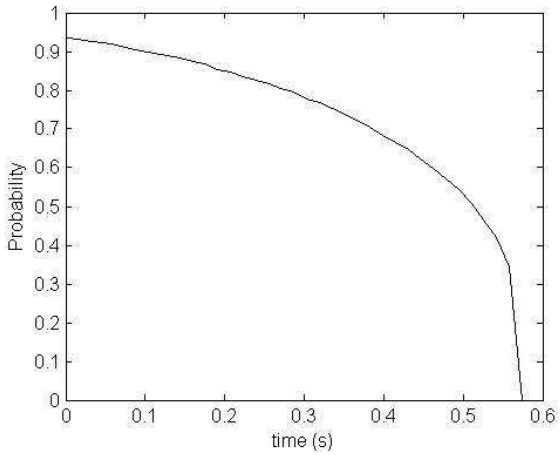

Fig. 7. Probability of coalescence when the second drop is deposited t seconds after the first drop has stabilized for water on glass.

V. Conclusion

This paper outlines the development of a coalescence model, which can be used as an image quality constraint in finding an optimal print mask. The proposed coalescence model computes the probability of coalescence as a function of time between two adjacent drops. Given an acceptable coalescence probability, the minimum printing time between adjacent drops can be determined, which translates to a minimum distance between pixels in a print mask that can be printed on the same pass. Additional experiments are needed to validate this theory.

Acknowledgment

The authors would like to thank the Hewlett Packard Company for providing the thermal inkjet drop ejection system for this study, Epoxies Etc. for providing epoxy used in the experiments, Keyence for providing the sample images for drop distribution characterization, James A. Mynderse for helpful discussions, and Raymond A. Decarlo for motivational conversations.

REFERENCES

[1] P. Calvert, "Inkjet Printing for Materials and Devices," *Chem. Mater.*, vol. 13, no. 10, pp. 2399–3305, 2001.

[2] N. J. Post, *Precision Micro – Deposition of Functional Layers Using Inkjet Drop – On Demand and Applications to the Functionalization of Microcantilever Sensors*, Thesis, Purdue University, 2007.

[3] W. Boley, "Inkjet Printing Involving Palladium Alkanethiolates and Carbon Nanotubes Functionalized with Single-Strand DNA," Proc. of *IS&T NIP25*, 2009.

[4] E. R. Lee, *Microdrop Generation*. New York, NY: CRC 2003, pp. 18-19.

[5] J. Yen, "Constraint Solving for Inkjet Prink Mask Design," *Journal of Imaging Science and Technology*, vol. 44, no. 5, pp. 391-397, Sep./Oct. 2000.

[6] J. Yen, "Improved Print Masks for Inkjet Printers," *U.S. Patent* 5,992,262, 1999.

[7] J. M. Garcia, "On the Design of Print Masks," Internal Report, IJBU-Barcelona, Hewlett-Packard Co., 1997.

[8] R. Rioboo, "Outcomes from a Drop Impact on Solid Surfaces," *Atomization and Sprays*, vol. 11, pp. 155-165, 2001.

[9] P. Attané, "An Energy Balance Approach of the Dynamics of Drop Impact on a Solid Surface," *Physics of Fluids*, vol. 19, 2007.

[10] A. Mongruel, "Early Post-Impact Time Dynamics of Viscous Drops onto a Solid Dry Surface," *Physics of Fluids*, vol. 21, 2009.

[11] R. Kannan, "Impact of Liquid Drops on a Rough Surface Comprising Microgrooves," *Exp. Fluids*, vol. 44, pp.937-938, 2008.

[12] H.-Y. Kim, "The Recoiling of Liquid droplet Upon Collision with Solid Surfaces," *Physics of Fluids*, vol. 13, no. 3, pp. 643-659, 2001.

[13] G. German, "Review of Drop Impact Models and Validation with High-Viscosity Newtonian Fluids," *Atomization and Sprays*, vol. 19, no. 8, pp. 787-807, 2009.

[14] G. Desie, "Multiple Drop Interactions with Substrates," Proc. of *IS&T NIP19*, 2003.

[15] M. Pasandideh-Fard, "Capillary Effects During Droplet Impact on a Solid Surface," *Physics of Fluids*, vol. 8, no. 3, pp. 650-659, 1996.

[16] A. Golpaygan, "Numerical Investigation of Impact and Penetration of a Droplet onto a Porous Substrate," *Journal of Porous Media*, vol. 11, no. 4, pp. 323-341, 2008.

[17] I. V. Roisman, "Normal Impact of a Liquid Drop on a Dry Surface: Model for Spreading and Receding," *Proc. of the Royal Society London A*, vol. 458, pp. 1411-1430, 2002.

[18] C. D. Stow, "An Experimental Investigation of Fluid Flow Resulting from the Impact of a Water Drop with an Unyielding Dry Surface," *Proc. of the Royal Society London A*, vol. 373, pp. 419-441, 1981.

[19] A. L. Yarin, "Drop Impact Dynamics: Splashing, Spreading, Receding, Bouncing…," *Annu. Rev. Fluid Mech.*, vol. 38, pp. 159-192, 2006.

[20] X. Zhang, "Dynamic Surface Tension Effects in Impact of a Drop with a Solid Surface," *Journal of Colloid and Interface Science*, vol. 187, pp. 166-178, 1997.

[21] R. G. Picknett, "The Evaporation of Sessile or Pendant Drops in Still Air," *Journal of Colloid and Interface Science*, vol. 61, no. 2, pp. 336-350, 1977.

[22] J. P. Hecht, "Spray Drying: Influence of Developing Drop Morphology on Drying Rates and Retention of Volatile Substances. 2. Modeling," *Ind. Eng. Chem. Res.*, vol. 39, pp. 1766-1774, 2000.

[23] H. Y. Erbil, "Drop Evaporation on Solid Surfaces: Constant Contact Angle Mode," *Langmuir*, vol. 18, pp. 2636-2641, 2002.

[24] H. Hu, "Evaporation of a Sessile Droplet on a Substrate," *J. Phys. Chem. B*, vol. 106, pp. 1334-1344, 2002.

[25] K. Sefiane, "Experimental Study of Evaporating Water-Ethanol mixture Sessile Drop: Influence of Concentration," *International Journal of Heat and Mass Transfer*, vol. 46, pp. 4527-4534, 2003.

[26] E. Bernal, "Improved Pen Alignment for Bidirectional Printing," *Journal of Imaging Science and Technology*, vol. 51, no. 1, pp. 1-22, 2007.